Proceedings of the Canadian Society for Mechanical Engineering International Congress
32nd Annual Conference of the Computational Fluid Dynamics Society of Canada
Canadian Society of Rheology Symposium
CSME-CFDSC-CSR 2025
May 25–28, 2025, Montréal, Québec, Canada

Computational Thermodynamics Approach to Overcoming Challenges in High-Nitrogen Low-Manganese Stainless Steel Production

Manel Houria[1], Kianoosh Kaveh[1], Jean-Benoit Morin[2], Mohammad Jahazi[1], Elmira Moosavi-Khoonsari[1*]
[1] Department of Mechanical Engineering, École de technologie supérieure (ÉTS), Montréal, Québec, Canada
[2] Finkl Steel-Sorel Inc, Sorel-Tracy, Québec, Canada
*Elmira.moosavi@etsmtl.ca

Abstract— The addition of nitrogen (N) to low-manganese (Mn) stainless steel significantly enhances its properties. However, producing high-N steel presents challenges, including N volatilization and casting system clogging. A strong foundation in thermodynamics is critical for understanding the direction and extent of chemical reactions under varying conditions. Building on thermodynamics, reaction kinetics provide insight into deviations from equilibrium. Experimental approaches, whether at the laboratory or pilot scale, are often time-intensive and costly. Computational thermodynamics offers an efficient alternative to address complex chemical reactions and interactions, particularly in high-temperature processes involving multicomponent systems and various operational parameters, where equilibrium is either local or global. This study applies computational thermodynamics to address challenges in producing high-N, low-Mn stainless steel in a scrap-based electric arc furnace route. It investigates the FeMnN addition to steel melt and explores potential causes of clogging in the nozzle and slide gate system during casting. Industrial measurements are incorporated to ensure the validity of the computational predictions.

Keywords- Electric arc furnace, scrap-based steelmaking, high nitrogen stainless steel, casting system clogging, thermodynamic calculations

I. INTRODUCTION

Adding a sufficient amount of nitrogen (N) (<1wt%) to a certain series of stainless steels contributes to the improvement of numerous properties, such as corrosion resistance, strength, creep strength, and toughness [1-3]. In some cases, N can act as an austenite stabilizing element, replacing Ni and thereby reducing the cost of steelmaking [1-3]. However, several challenges arose during the addition of N and the casting process in the production of this steel via the scrap-based electric arc furnace (EAF) route. Nitrogen volatilization occurred at process temperatures (1650 °C) during the degassing stage, resulting in the loss of most of the added N. Moreover, during the casting of high-N, low-manganese (Mn) stainless steel, nozzle clogging occurred, preventing the completion of production. An empirical approach was unsuccessful due to the lack of prior experience in producing this specific grade of steel.

Experimentation, whether on a lab scale or pilot scale, is both time-consuming and costly. Real-scale experiments, without proper knowledge of the impact of new modifications, present challenges such as process interruption, the risk of breakout, and production delays. Alternatively, thermodynamic simulation and modeling can provide direct and deeper insight into specific problems of processes [4-6], followed by key lab-scale experiments or plant trials for validation.

Various self-consistent and accurate thermodynamic databases have been developed in the past decades as solutions for a wide range of applications, incorporated into computational thermodynamic software equipped with Gibbs energy minimizers such as FactSage [7], Thermocalc [8]. These thermochemical packages can be employed to perform the thermodynamic assessment of a chemical system. In this work, we illustrate the utilization of thermodynamic calculations in addressing real process challenges in the production of high N - low Mn stainless steel in a scrap-based EAF steelmaking.

II. COMPUTATION-BASED PROBLEM-SOLVING APPROACH

The thermodynamic analysis was performed using FactSageTM version 8.2 thermochemical software [7]. FactSage and its specialized databases have been applied to different applications such as steelmaking [4,6,9,10], non-ferrous production [10-13], glassmaking [14], and recycling [15,16] in high-temperature materials processing [17,18]. The Gibbs free energy minimization algorithm, allow us to calculate the phase equilibria and complex chemical reactions between metal, slag and gas under a set of predefined conditions (e.g., composition, temperature, pressure, oxygen partial pressure). It comprises various modules, with a primary focus on the Equilib and Phase Diagram modules in this study.

Thermodynamic descriptions of the slag (solid and liquid) were taken from the FToxid database. The steel phase was modeled using FSstel or FTmisc databases, depending on the

Identify applicable sponsor/s here. *(sponsors)*

application (the former is preferred for calculations involving steel solidification while the latter is employed for steel refining). The thermodynamic behavior of the gas phase was modeled using the FactPS database and the refractory linings, including oxides and graphite components, using both FToxid and FactPS, respectively.

III. Production of High-Nitrogen - Low Mn Stainless Steel

A. *Thermochemical simulation of FeMnN addition*

Fig. 1 illustrates the effect of FeMnN addition on steel N and Mn contents at 1650 ºC. The black lines on Fig. 1a correspond to initial N contents of 200 ppm and 230 ppm in the base steel melt, and the symbols present the measured N content of steel collected during the plant trial. The black lines on Fig. 1b correspond to initial Mn contents in steel of 0.15, 0.22, 0.31, and 0.45 wt% and the symbols show the measured steel Mn content.

As seen in Fig. 1a, after addition of a total of 340 kg of FeMnN, a N concentration of 375 ppm was reached, which was not the desired target (Mn content reached 0.93 wt%). According to the thermochemical calculations, having about 200 ppm of N in base steel and exceeding the target N of 600 ppm in final steel, the total mass of FeMnN to be added to steel was determined to be about 450 kg FeMnN (considering 100% efficiency for N).

Moreover, considering the added amount of FeMnN, and the maximum target value of Mn in steel, the required initial Mn content of steel melt before any FeMnN addition was calculated. According to thermochemical calculations and mass balance between steel melt, slag, and gas, it is necessary to have a base melt composition with a maximum of ~0.2% Mn, as shown in Fig. 1b, which can be adjusted during EAF-LF operation.

In addition, according to the measurements, after the first addition of FeMnN in steel (at the end of LF), the target N concentration in steel was not achieved. The N amount was 360 ppm (the Mn amount was 0.75 wt%). Additionally, after the degassing step, the N amount in the steel further dropped to 218 ppm. During VAD, N scaped the melt (no change occurred in Mn concentration of steel). N vaporization was reported as a challenge [3]. For increasing the N amount in steel composition, as a second step, approximately 113 kg of FeMnN was added to the steel after the degassing step. Therefore, thermodynamic calculations were done to understand the effect of vacuum on the N solubility in steel during the degassing step.

Fig. 2 illustrates the effect of degassing pressure on N solubility. In the equilibrium state, the vacuum can decrease the solubility limit of N from ~140 ppm to ~35 ppm for 9 and 1 mbar pressure, respectively. Thus, if the vacuum degassing was prolonged for enough time, the N content would have dropped even lower after the first addition of FeMnN, i.e., from 218 ppm to below ~140 ppm in the equilibrium state. The calculated effect of vacuum negative pressure on the N removal from steel is in accordance with the plant data. This confirms that the FeMnN additions should be performed after vacuum degassing to reach the target composition of ~600 ppm of N. Therefore, it is important to determine the best moment for the addition of the FeMnN.

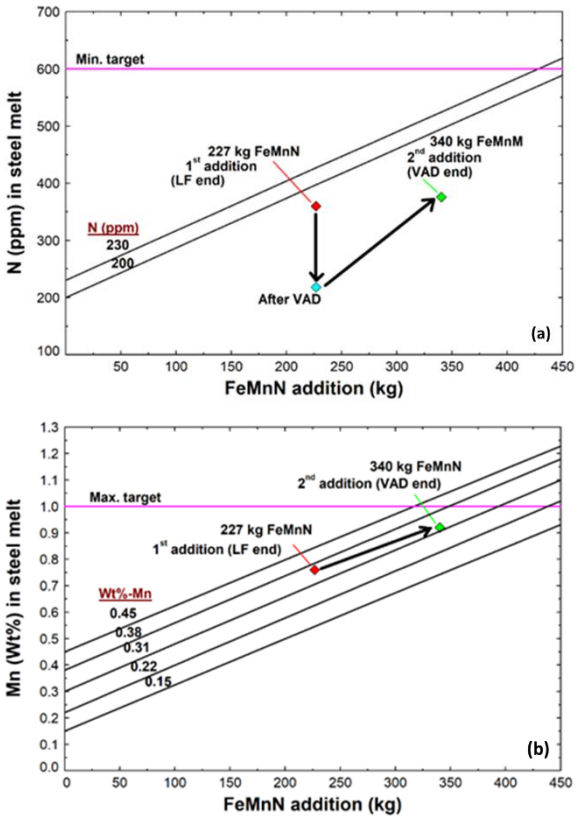

Figure 1. Effect of FeMnN addition on final (a) N content and (b) Mn content of steel, calculated for different initial N and Mn contents of steel along with plant data as symbols (at 1650 ºC).

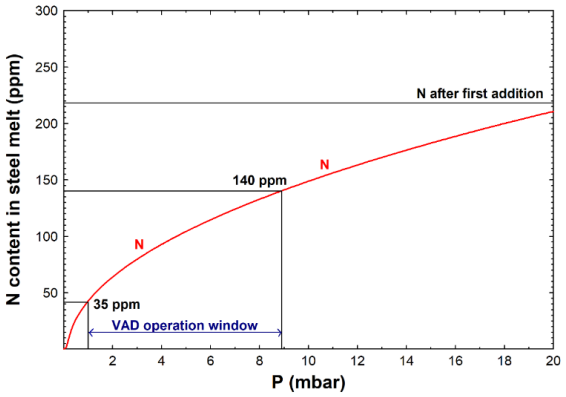

Figure 2. Effect of degassing negative pressure on N solubility in steel, calculated at 1600 ºC.

During vacuum degassing step, bath agitation by Ar gas is conducted, which could affect the steel composition. For this reason, a thermochemical calculation was carried out to understand the effect of the bath stirring by Ar(g) on the steel N and Mn contents. The calculations were performed under an open system condition (i.e., the inlet gas is refreshed, and outlet gas can exit the system) to simulate the effect of Ar flow through the system on the N and Mn stability in steel.

Fig. 3 shows the effect of Ar injection (5 l/min) on the partial pressure of gaseous species in the outlet gas. The results shows that the N behavior is constant. That is, Ar does not affect the equilibrium thermodynamic behavior of N in steel. It only accelerates the kinetics of N removal. The above findings are in

agreement with those reported by Ardelean et al. [19] who showed that raising the temperature of liquid steel from 1600 to 1650 ºC during LF treatment lowers the steel's viscosity. This, in turn, facilitates the diffusion of N from the steel into the Ar bubbles, reduces the resistance to movement of the Ar bubbles, and contributes to N removal. Moreover, according to the calculations, the Mn concentration of steel and therefore, the Mn vapor pressure in the gas phase remains constant during Ar injection after the vacuum degassing step.

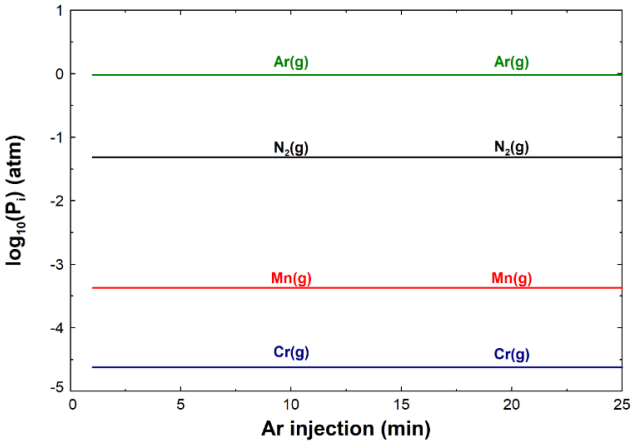

Figure 3. Effect of Ar injection on the composition of outlet gas, calculated at 1600 ºC.

B. *Clogging of nozzle / slide gate casting system*

After addition of FeMnN during stainless steel production, the nozzle clogging was noticed during casting which is a common industrial problem [20-21]. For further details, following the vacuum degassing step, to cast the steel in the mold, the ladle is placed on the casting system, comprising refractory-lined nozzles and a sliding gate. The buildup of material in the flow passage of the molten steel during casting was observed after the FeMnN addition, but the nature of the buildup and its causes were not clear. Additionally, the casting system is essentially permanent and cannot be removed for microstructural characterization.

Fig. 4 depicts a schematic representation of the nozzle/slide gate system design, comprising three types of refractories. 'Component 1' is made of alumina-magnesia refractory, 'Component 2' is made of alumina-silicate refractory, and 'Component 3' is made of alumina-silicate-carbon bonded refractory.

Rackers et al. [22] reported that clogging can take several forms, including the agglomeration of complex oxide and sulfide inclusions and/or the buildup of solid steel. The causes of clogs are attributed to turbulent recirculation zones, turbulent flow, and roughness of nozzle walls and corners [22]. They recommended preventing clogging by improving steel cleanliness. For instance, vacuum degassing was found to produce cleaner steel compared to Ar bubbling [22]. Clogging due to Nitrides [20,23] et due to steel/nozzle reactions [22]. Furthermore, Wen et al. [20] announced three factors which can affect the formation of nozzle clogging. The first one is the physical adhesion of high-melting-point inclusions, the second factor is the temperature drop resulted from the insufficient preheating of nozzles and the temperature fluctuation of molten steel, and finally, the chemical reactions occur during the continuous casting.

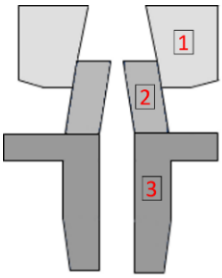

Figure 4. Schematic representation of nozzle / slide gate casting system

C. *Thermochemical calculations to understand the clogging root-causes*

The goal of the thermochemical calculations was to comprehend the nature of the build-up and propose a solution. Therefore, based on Rackers et al. [22] the clogging can be caused by refractory reactions with steel and the accumulation of oxide scales in the nozzle/slide gate system. Furthermore, according to our case study and the literature [20,22-24], several hypotheses were formulated as probable causes of clogging due to the addition of FeMnN to steel: (a) an increase in the new steel liquidus temperature leading to steel buildup, (b) the formation of nitride and sulfide inclusions [20-23], and (c) changes in the solubility limit of oxygen in the steel and precipitation of oxide inclusions [24]. Systematic thermochemical calculations were conducted to validate or dismiss each hypothesis, as elaborated below.

a) Increase in new steel melting temperature during casting. The first hypothesis posited that the increase in the liquidus temperature of newly cast high-N steel resulted in partial steel solidification on the nozzle/slide gate system, leading to clogging. Therefore, the liquidus temperature of various steel compositions was calculated based on the addition of varying amounts of FeMnN.

Fig 5 illustrates the effect of FeMnN addition on the liquidus temperature of the melt. The results indicate that the liquidus temperature slightly decreased with the addition of FeMnN. Specifically, an addition of 113 and 227 kg of FeMnN decreased the liquidus temperature from 1520 °C to 1510 °C, while an addition of 340 and 454 kg further decreased it to 1500 °C. In other words, there was a slightly higher superheat available for high-N steel compared to the base steel with low N content. Therefore, partial solidification of steel could not be attributed as the cause of the clogging in the casting system.

b) Formation of nitride and sulfide inclusions. The question arose regarding the stability of nitrides at process temperatures or their precipitation during the solidification of steel during casting [20-23]. Therefore, the temperature-N (T-N) phase diagram of the final steel composition was calculated to illustrate the phase stability versus temperature.

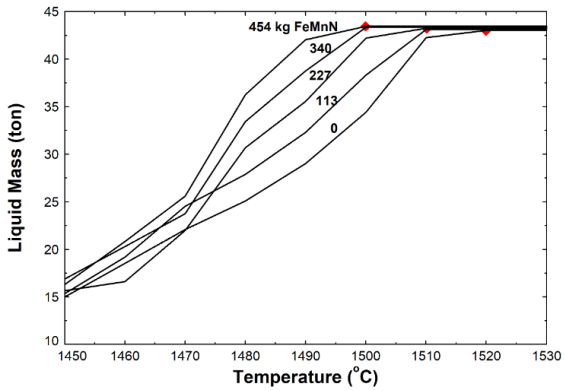

Figure 5. Calculated effect of FeMnN addition on the liquidus temperature of the steel melt.

Fig. 6 displays the phase diagram of the steel as a function of its N content at different temperatures, ranging from high process temperature to solidification. The chemical composition of the steel after the second addition of N is represented by the pink vertical line on the phase diagram, depicting the equilibrium solidification path from above the liquidus temperature (~1490 °C, red line) down to 900 °C. Calcium sulfide (CaS) forms from the interaction between lime (CaO) and sulfur (S) in steel at process temperature. For the high-N steel composition, at 1490 °C, delta ferrite (BCC) precipitates out from the liquid metal, and then at 1380 °C, austenite (FCC) precipitates from the liquid phase. Upon cooling to temperatures below 1380 °C (blue line), all the liquid metal solidifies. As indicated, aluminum nitride (AlN) phase is not stable at processing temperatures, and the precipitation of AlN only occurs at temperatures much below the end of steel solidification, specifically at temperatures lower than 1100 °C for all N contents in the studied range.

The formation of AlN occurs as a result of the reaction between Al and N in steel:

$$2Al + N_2(g) = 2AlN \quad (1)$$

Upon cooling and during solidification, as the solubility limits of Al and N decrease in steel, the reaction between Al and $N_2(g)$ occurs. In addition, low temperatures favor the reaction (1) and the formation of AlN. The equilibrium constant (Keq) of this reaction as a function of temperature is shown in Fig. 7:

$$\log K_{eq} = -5.7948 + 16751/T\ (K) \quad (2)$$

The N solubility is also affected by the chemical composition of the steel [2,25]. While some alloying elements (e.g., S, Al, C, Co, Cu, Ni, Si and O) decrease the solubility of N [25,26], some others such as Mn, Cr, Mo, Ta, W, and V increase it [26].

In liquid steel at 1650 °C (at the process temperature), the maximum solubility of N in steel is calculated to be 1650 ppm, with no nitride precipitation. At 1490 °C (just above the liquidus temperature), the solubility limit of N in the melt increases to 1850 ppm. At 1390°C (just above the solidus temperature), 3020 ppm of N can dissolve in the remaining liquid, FCC uptakes a maximum of 1340 ppm, and the δ-BCC dissolves about 380 ppm. At 1010 °C, the N solubility in the FCC phase increases to 2043 ppm, where the formation of AlN begins (aAlN = 1.0). At room temperature, less than 10 ppm of N dissolves in the ferrite (BCC) phase [25]. Thermochemical calculations implied that the accumulation of AlN on the nozzle refractories cannot occur during the pouring of the steel, and AlN could not have caused the clogging issue.

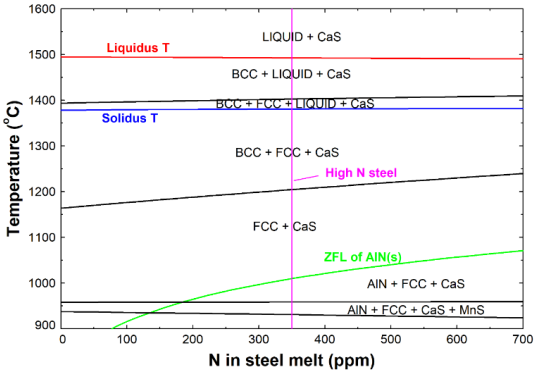

Figure 6. Calculated temperature-nitrogen phase diagram and nitride formation (ZFL: zero fraction line).

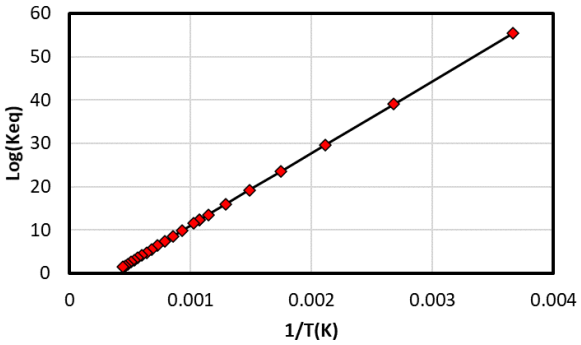

Figure 7. Calculated log(Keq) of AlN formation from the steel melt as a function of 1/T(K).

(c) Change in the solubility limit of oxygen in steel (oxide inclusions). Another hypothesis reported that the addition of elevated levels of N and a comparatively higher Mn content to the steel would decrease the solubility limit of O in steel, leading to the formation of oxides. Such oxides could potentially cause the observed clogging [24]. This calculation allows for considering the effect of N and Mn concentrations on O solubility in steel after LF refining, as indicated by the oxide formation.

Fig. 8 depicts the mass of oxide inclusions as a function of N content in steel at 1580 ºC, calculated for four base steel compositions (0.2 wt% Mn and 100 ppm O; 1 wt% Mn and 100 ppm O; 0.2 wt% Mn and 50 ppm O; 1 wt% Mn and 50 ppm O). The temperature of 1580 °C corresponds to the steel temperature after VAD, just before casting. The chosen Mn concentrations aim to facilitate a comparison between the quantity of oxide inclusions in the base steel composition before the addition of FeMnN and the target steel composition after incorporating FeMnN. The predominant solid inclusions include $CaAl_4O_7$ (CAF2), $CaAl_{12}O_{19}$ (CAF6), Al_2O_3 (CORU), $(Mn,Cr)Al_2O_4$ (TSpi).

As observed in Fig. 8, increasing the steel N content does not largely change the O solubility in steel however, the elevation in Mn content at high N levels reduces the oxygen solubility in

steel, leading to the formation of more oxide inclusions, particularly CAF2 and TSpi. When the steel contains only 50 ppm O, there is no substantial change in the mass and composition of oxide inclusions with an increase in the alloying element content of the steel because the O content of steel is far from the saturation limit. Fig. 9 depicts the evolution of oxide inclusion composition from the calcium aluminoferrite ($CaAl_{12}O_{19}$) in the base steel to $CaAl_4O_7$ and Spinel as a result of FeMnN addition and an increase in MnO content. Consequently, the increased formation of oxide inclusions in steel with a higher content of alloying elements at the process temperature (i.e., 1580 °C) may contribute to potential clogging in the nozzle/slide gate system.

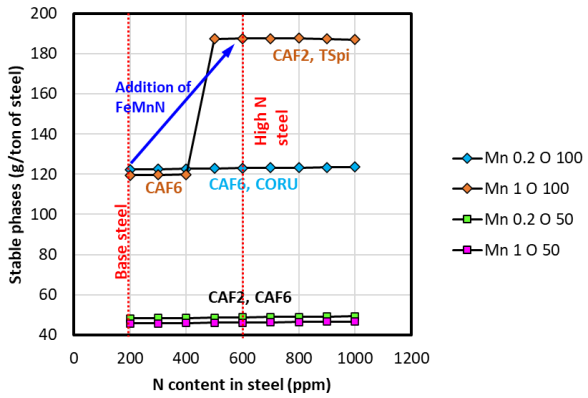

Figure 8. Oxide inclusions in steel melt as a function of steel N content, calculated for various initial Mn and O contents of steel at 1580 °C. x and y in Mn x O y stand for wt% of Mn and ppm of O in base steel, respectively. CAF2, CAF6, CORU, TSpi stand for $CaAl_4O_7$, $CaAl_{12}O_{19}$, Al_2O_3, and $(Mn,Cr)Al_2O_4$, respectively.

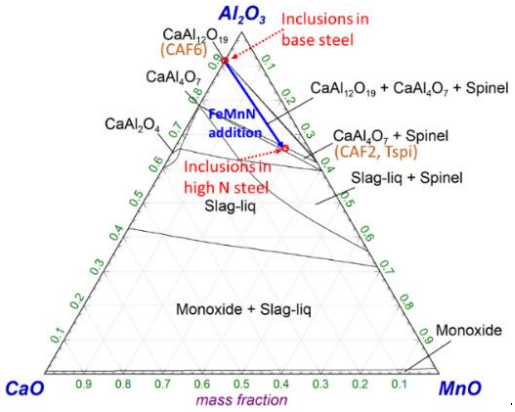

Figure 9. Composition evolution of nonmetallic inclusions with the addition of FeMnN, calculated at 1580 °C and $P_{O2}=10^{-13}$ atm.

In addition, another hypothesis has been postponed by Rackers et al. [22] is taken into consideration.

d) Refractory/steel interactions and scale buildup on the casting system. The final hypothesis considers interfacial reactions occurring between the flowing steel stream and the refractories of the slide-gate/nozzle lead to the formation and accumulation of accretions inside the nozzle. Consequently, the free path for the flow of steel becomes progressively constricted, ultimately leading to the occurrence of clogging.

Counter-flow diagrams utilizing the variable <A> (representing the steel/refractory mass ratio entering the reaction) were employed to simulate the refractory-steel interface. The parameter <A> varied within the range of 0 to 1.0, where '0' signifies the bulk refractory, '1.0' represents the bulk steel, and any values in between denote the steel-refractory interface. The chemistries and quantities of interaction products present at the interface were subsequently investigated, encompassing all <A> values ranging from 0 to 1.0. The primary reaction products observed at the interface included $NaAl_9O_{14}$, $CaFe_6Al_2O_{10}$, $CaMg_2Al_{16}O_{27}$, $Ca_2Mg_2Al_{28}O_{46}$, tetragonal ZrO_2, and Al_2O_3.

Fig. 10 illustrates the mass gain at the high alloy steel/nozzle interface with respect to the base low alloy steel, presented as a function of the steel/refractory mass ratio simulated for a 20-minute process, based on the amount of steel flow. The mass gain was computed using the following formula:

$$\%\ Mass\ gain = \left(\frac{Mass\ of\ Solids_{High\ alloy} - Mass\ of\ Solids_{Low\ alloy}}{Mass\ of\ Solids_{Low\ alloy}}\right) \times 100 \quad (3)$$

As shown in Fig. 10, upon comparing the mass gain percentage at each interface for various steel/refractory ratios and different components of the nozzle/slide-gate system, it becomes evident that the total amount of solids accumulated on the new steel side of the interface can increase by 2%, 16%, and 15% for 'Component 1' of the nozzle, 'Component 2' of the nozzle, and 'Component 3' of the slide-gate, respectively.

The mass increase is more pronounced for high MnN steel. As this process is cumulative, it can eventually lead to clogging. The highest mass gain was observed at the interface adjacent to steel. This increase in solid phases, particularly for 'Component 2' and slide gate 'Component 3,' may indicate a higher risk of accretion formation at the steel interface and a potential cause of clogging (note: the cumulative effect of other inclusions such as $CaAl_4O_7$ (CAF2) and $(Mn,Cr)Al_2O_4$ (TSpi) was not considered). Industrial validation showed that the lower nozzle, i.e., 'Component 3,' appeared to experience the most significant clogging, aligning with the thermodynamic calculations. As mentioned earlier, the clogged system was promptly cleaned after the operation, preventing the collection and microstructural investigation to further validate the hypothesis. One potential solution to this problem might be enlarging the nozzle size to prevent complete clogging just before achieving a mold full fill.

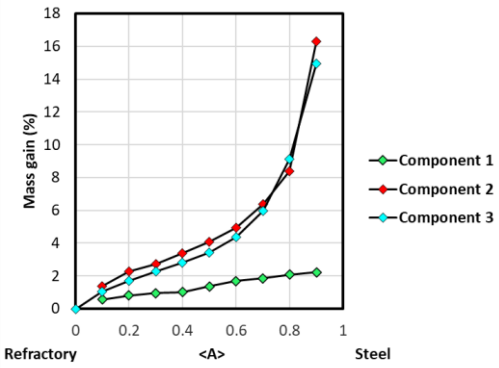

Figure 10. Calculated mass gain (with relation to low alloy steel) at the interface between high alloy steel and refractory components of nozzle/slide gate casting system.

IV. CONCLUSION

Computational thermodynamics facilitates a deeper comprehension of the thermochemical phenomena that govern an industrial-scale process and the underlying causes of problems. This study utilized thermodynamic calculations and simulations to address certain issues encountered at various stages of high N, low Mn stainless steel production. The key findings are summarized below:

It was proposed in this work and validated by industry to introduce FeMnN after vacuum degassing, followed by argon stirring, to prevent N loss during the process. This approach was applied in subsequent castings to produce the target N-steel. Additionally, the initial Mn content of the steel was adjusted to achieve the desired target values for both N and Mn in the steel.

In casting high Mn, N steel, clogging may occur due to increased levels of both steel/refractory chemical reactions and the formation of oxide inclusions ($CaAl_4O_7$ (CAF2), $CaAl_{12}O_{19}$ (CAF6), Al_2O_3 (CORU), $(Mn,Cr)Al_2O_4$ (TSpi), $NaAl_9O_{14}$, $CaFe_6Al_2O_{10}$, $CaMg_2Al_{16}O_{27}$, $Ca_2Mg_2Al_{28}O_{46}$, tetragonal ZrO_2, and Al_2O_3) due to decreased oxygen solubility in the melt, in contrast to steel with lower Mn and N content. Consequently, oxide and accretion buildup occur in the nozzle/slide gate casting system, leading to nozzle clogging. The calculations showed that nitrides could not be the clogging cause.

Thermochemical calculations helped the plant minimize risks during trials, lower experimental costs, and improve product quality. However, the reliability of these calculations depends on selecting appropriate thermodynamic databases, phases, and process variables. Additionally, kinetics must be considered, as equilibrium thermodynamics alone does not account for reaction rates.

ACKNOWLEDGMENT

The authors would like to acknowledge Finkl Steel-Sorel and Mitacs Accelerate Program (IT28458) for financial support of the project.

REFERENCES

[1] P. Machovčák, Z. Carbol, A. Opler, A. Trefil, J. Bažan, and L. Socha, "NITROGEN ALLOYING OF HIGH CHROMIUM STEELS BY GAS INJECTION IN THE LADLE," Acta Metallurgica Slovaca-Conference, vol. 4, pp. 152–159, 2014, doi: 10.12776/amsc.v4.220.

[2] Z. Jiang, H. Li, Z. Chen, Z. Huang, D. Zou, and L. Liang, "The nitrogen solubility in molten stainless steel," Steel Res Int, vol. 76, no. 10, pp. 740–745, 2005, doi: 10.1002/srin.200506090.

[3] A. Svyazhin, L. Kaputkina, I. Smarygina, and D. Kaputkin, "Nitrogen Steels and High-Nitrogen Steels: Industrial Technologies and Properties," Sep. 01, 2022, John Wiley and Sons Inc. doi: 10.1002/srin.202200160.

[4] I. H. Jung and M. A. Van Ende, "Computational Thermodynamic Calculations: FactSage from CALPHAD Thermodynamic Database to Virtual Process Simulation," Metallurgical and Materials Transactions B, vol. 51, no. 5, pp. 1851–1874, Oct. 2020, doi: 10.1007/s11663-020-01908-7.

[5] A. Costa e Silva, "Applications of Multicomponent Databases to the Improvement of Steel Processing and Design," J Phase Equilibria Diffus, vol. 38, no. 6, pp. 916–927, Dec. 2017, doi: 10.1007/s11669-017-0575-2.

[6] J. R. Castillo-Sánchez, K. Oishi, L. St-Germain, D. Ait-Amer, and J. P. Harvey, "The power of computational thermochemistry in high-temperature process design and optimization: Part 1 — Unit operations," CALPHAD, vol. 82, p. 102593, Sep. 2023, doi: 10.1016/j.calphad.2023.102593.

[7] C. W. Bale et al., "FactSage Thermochemical Software and Databases," Calphad, vol. 26, no. 2, pp. 189–228, 2002, [Online]. Available: http://www.crct.polymtl.cahttp://gttserv.lth.rwth-aachende

[8] J.-O. Andersson, T. Helander, L. Hoglund, P. Shi, and B. Sundman, "Thermo calc and DICTRA Computational Tools For Materials Science," Calphad, vol. 26, pp. 273–312, 2002.

[9] T. S. Prithiv, G. Thirumurugan, M. Madan, and A. Kamaraj, "Thermodynamic Assessment of Steelmaking Practices for the Production of Re-sulfur Steels," Transactions of the Indian Institute of Metals, vol. 73, no. 6, pp. 1595–1603, Jun. 2020, doi: 10.1007/s12666-020-01941-9.

[10] J. P. Harvey et al., "On the application of the FactSage thermochemical software and databases in materials science and pyrometallurgy," Processes, vol. 8, no. 9, Sep. 2020, doi: 10.3390/PR8091156.

[11] I. H. Jung, Z. Zhu, J. Kim, J. Wang, P. Chartrand, and A. Pelton, "Recent Progress on the Factsage Thermodynamic Database for New Mg Alloy Development," JOM, vol. 69, no. 6, pp. 1052–1059, Jun. 2017, doi: 10.1007/s11837-017-2331-9.

[12] S. Xie and B. Zhao, "Phase Equilibrium Studies of Nonferrous Smelting Slags: A Review," Metals (Basel), vol. 14, no. 3, p. 278, Feb. 2024, doi: 10.3390/met14030278.

[13] E. Moosavi-Khoonsari and S. Mostaghel, "Thermodynamic assessment of tin-smelting from cassiterite concentrates," Canadian Metallurgical Quarterly, pp. 1–14, 2023, doi: 10.1080/00084433.2023.2266209.

[14] L. I. P. Baccarin, W. V. Bielefeldt, and S. R. Bragança, "Prediction of glass phase viscosity in firing traditional ceramics and porcelain tiles with waste glass powder," Open Ceramics, vol. 15, p. 100417, Sep. 2023, doi: 10.1016/j.oceram.2023.100417.

[15] Y. Qu, K. Tan, B. Zhao, and S. Xie, "Recovery of Cu-Fe Alloy from Copper Smelting Slag," Metals (Basel), vol. 13, no. 2, p. 271, Feb. 2023, doi: 10.3390/met13020271.

[16] Z. Zulhan and N. Agustina, "A novel utilization of ferronickel slag as a source of magnesium metal and ferroalloy production," J Clean Prod, vol. 292, p. 125307, Apr. 2021, doi: 10.1016/j.jclepro.2020.125307.

[17] L. Xu and B. Zhao, "Extraction of Sodium Tungstate from Tungsten Ore by Pyrometallurgical Smelting," Metals (Basel), vol. 13, no. 2, p. 312, Feb. 2023, doi: 10.3390/met13020312.

[18] M. Sommerfeld, J. Weiss, and B. Friedrich, "CO2-Minimized Ferrochrome Production Utilizing Silicon Wafer Cutting Slurry as an Alternative Reductant," Journal of Sustainable Metallurgy, vol. 9, no. 2, pp. 806–815, Jun. 2023, doi: 10.1007/s40831-023-00688-z.

[19] E. Ardelean, M. Ardelean, A. Josan, and C. Pinca-Bretotean, "Contribution on the influence of steel ladle processing (LF) upon the nitrogen removal rate," IOP Conf Ser Mater Sci Eng, vol. 57, no. 1, p. 012001, 2014, doi: 10.1088/1757-899X/57/1/012001.

[20] W. Yang, L. Zhang, Y. Ren, W. Chen, and F. Liu, "Formation and Prevention of Nozzle Clogging during the Continuous Casting of Steels: A Review," ISIJ International, vol. 64, no. 1, pp. 1–20, Jan. 2024, doi: 10.2355/isijinternational.isijint-2023-376.

[21] B. Harcsik, P. Tardy, and G. Karoly, "Examination of nozzle clogging in continuous casting," Revue de Metallurgie. Cahiers D'Informations Techniques, vol. 109, no. 3, pp. 177–186, 2012, doi: 10.1051/metal/2012046.

[22] K. G. Rackers and B. G. Thomas, "Clogging in Continuous Casting Nozzles," Iron and Steel Society, Warrendale, PA , vol. 78, pp. 723–734, 1995.

[23] J. Burja, M. Koležnik, Š. Župerl, and G. Klančnik, "Nitrogen and nitride non-metallic inclusions in steel," Materiali in Tehnologije, vol. 53, no. 6, pp. 919–928, 2019, doi: 10.17222/mit.2019.247.

[24] J. Li, G. Cheng, Q. Ruan, J. Pan, and X. Chen, "Characteristics of Nozzle Clogging and Evolution of Oxide Inclusion for Al-Killed Ti-Stabilized 18Cr Stainless Steel," Metallurgical and Materials Transactions B: Process Metallurgy and Materials Processing Science, vol. 50, no. 6, pp. 2769–2779, Dec. 2019, doi: 10.1007/s11663-019-01708-8.

[25] S. Yu, J. Miettinen, and S. Louhenkilpi, “Modeling study of nitrogen removal from the vacuum tank degasser,” Steel Res Int, vol. 85, no. 9, pp. 1393–1402, 2014, doi: 10.1002/srin.201300262.

[26] E. C. Young and A. Mitchell, “Some Aspects of Nitrogen Addition and Removal During Special Melting and Processing of Iron and Nickel Base-Alloys,” High Temperature Materials and Processes, vol. 20, no. 2, pp. 79–102, 2001.